Balancing power production and coastal protection: A bi-objective analysis of Wave Energy Converters

Renewable Energy 220 (2024) 119702

Contents lists available at ScienceDirect

Renewable Energy

journal homepage: www.elsevier.com/locate/renene

Balancing power production and coastal protection: A bi-objective analysis of Wave Energy Converters

Beatrice Battisti [a,b,*], Giuseppe Giorgi [a], Gael Verao Fernandez [c]

[a] Marine Offshore Renewable Energy Lab, Department of Mechanical and Aerospace Engineering, Politecnico di Torino, Turin, Italy
[b] Bordeaux Mathematical Institute, Université de Bordeaux, Talence, France
[c] Department of the Built Environment, Aalborg University, Aalborg, Denmark

ARTICLE INFO

Keywords:
Wave energy converter
Power production
Coastal protection
WEC farms
Power take-off

ABSTRACT

Wave Energy Converters (WECs) have the potential to serve dual purposes, generating power and protecting coastlines. Although traditionally the focus has been on maximizing power generation for cost-effectiveness, growing impacts of climate change have made coastal protection increasingly imperative. However, power production and coastal protection have been addressed separately, missing potential synergies. This paper addresses this gap by conducting a bi-objective analysis to investigate the interactions between power extraction and wave attenuation for a single Oscillating Surge Wave Converter (OSWC) and WEC farms of three and five units.

A linear Power Take-Off (PTO) system, with passive and reactive control strategies, is examined. By varying the PTO parameters, we assess their influence on both power production and wave field attenuation. Results demonstrate a significant impact of the PTO choice on wave attenuation, with a similar trend observed for power production. This finding highlights the potential for a trade-off, where maximizing wave attenuation may come at the cost of moderate energy output. Furthermore, the interactions observed within the WEC farms enhance this trend.

The study emphasizes the importance of a holistic approach to WEC technology development, promoting sustainable and resilient harnessing of wave energy resources, considering both power generation and coastal protection.

1. Introduction

In recent years, the importance of offshore renewable energy sources in achieving net zero energy targets and complete decarbonization has become evident, since they can complement and diversify a resilient energy mix [1]. Offshore wind is expected to contribute significantly to the installed capacity, while Wave Energy Converters (WECs) are envisioned to provide a more reliable and stable base load, thus reducing the demand for energy storage [2]. This has prompted both policymakers and the industry to focus on enhancing knowledge about array configurations of floating WECs [3].

On the one hand, the rated power of an individual WEC is usually relatively small, compared to grid requirements or other renewable energy plants, such as offshore wind turbines; on the other hand, WECs are normally costly for both the capital (CapEx) and operational (OpEx) expenditures [4]. Therefore, it is usually convenient to group WECs in farms [5], in order to leverage cost sharing, including CapEx reduction of the electric infrastructure and cable connection to the grid, and potentially shared mooring system, as well as convenient optimization of operational expenditure for planned or corrective maintenance.

The primary and most evident objective of a wave energy farm and its design process is to maximize the overall power absorption while simultaneously minimizing the levelized cost of energy (LCoE). Minimizing costs is closely related to reducing the overall footprint of the farm, as WECs installed further apart would require longer cable connections and potentially higher operational expenses. Therefore, it is generally reasonable to expect that minimizing costs also involves minimizing the overall distance between WECs. However, wave–structure interactions introduce complex modifications to the wave field surrounding each WEC, caused by diffraction and radiation effects. As a result, finding the optimal WEC–WEC coupling layout is often challenging and not intuitive. In fact, depending on the characteristics of both the floaters and the waves, alternating regions of destructive and potentially constructive interactions can be observed. Moreover, the WEC–WEC influence is affected by the farm layout: in [6], the power production of a farm over a range of inter-device

* Corresponding author at: Marine Offshore Renewable Energy Lab, Department of Mechanical and Aerospace Engineering, Politecnico di Torino, Turin, Italy.
E-mail addresses: beatrice.battisti@polito.it (B. Battisti), giuseppe.giorgi@polito.it (G. Giorgi), gvf@build.aau.dk (G.V. Fernandez).

https://doi.org/10.1016/j.renene.2023.119702
Received 1 August 2023; Received in revised form 4 November 2023; Accepted 19 November 2023
Available online 20 November 2023

distances is evaluated in realistic wave climates. The authors find that small distances and large array sizes enhance destructive interactions and thus, power loss.

A typical metric to quantify the performance of a farm, compared to a single WEC, is the so-called q-factor [7]: it is defined as the ratio between the actual productivity and the idealized case where interactions are neglected; therefore, the higher the q-factor the better, where $q > 1$ stands for constructive synergy. Most of the body of research in this topic concerns methods to optimize the q-factor by conveniently modifying the farm layout, in space and potentially number of devices, while including techno-economic metrics (e.g., cost of the electric cable [8]) and boundary constraints (e.g., minimum and maximum allowable distance between devices [9] or predefined reciprocal structure [10]). Genetic algorithms are a popular choice to handle such a complex multi-variate problem, since the dimension of the state vector to be optimized is normally too large for an exhaustive search [11,12].

In addition to layout optimization, recently attention has been drawn also on the energy-maximization control problem [13] of a farm, where centralized, distributed and decentralized approaches are shown to differ significantly and impact the overall productivity of the farm. An open access dataset has also been provided, related to a wave tank experimental campaign with up to 5 WECs [14].

Besides renewable energy production, a secondary beneficial effect of a WEC farm is to contribute to coastal protection [15]; indeed, coastal erosion is becoming a growing concern, partly driven by the effects of climate change [16]. Current state of the art solutions [17] encompass groynes, breakwaters, or barriers, which may present one or more of the following drawbacks: impact on marine life, turbidity, lagoon effects, danger to bathers, visual impact, among others. WECs offer the potential to mitigate some of such issues, since they do have the ability to modify the wave field in their lee: although local increases in wave height are possible, especially close to the floating devices due to the radiated waves, an overall attenuation is obtained.

Although usually seen just as a secondary result, normally overshadowed by energy production, the coastal protection by-product of WEC farms may be the decisive factor in the decision-making process. Indeed, given the substantial costs associated with coastal erosion and damage, incorporating WEC farms into the coastal protection strategy can lead to a reduction in wear on existing structures, minimize erosion, and lower associated risks. This cost synergy is essential in decreasing overall expenditure while increasing value, ultimately enhancing the economic viability of WECs [5].

In literature, several studies quantify the wave attenuation ability of a farm of WECs, usually considering overtopping or flap-type WECs [18]. In a technology-agnostic study carried out by [19], various transmission coefficients were utilized to simulate scenarios ranging from the absence of wave energy absorption to the ideal case of full absorption by the farm. It is important to highlight that it is common to simplify the wave–WEC interaction problem with a trivial transmission coefficient within far-field approaches, such as the spectral model used in [19], since the effectiveness of a WEC in absorbing energy is closely linked to its transmission coefficient [20]. A similar approach is used by [21] to simulate an overtopping device, modeling it as a circular obstacle with constant reflection and transmission coefficients. Some sensitivity analysis is performed in [22], where the role of the distance from shore of a given farm of overtopping is analyzed and discussed. To overcome the simplification of the wave–WEC interaction, [23] uses a model coupling a BEM solver for the near-field and a wave propagation model for the far-field. The authors evaluated the wake effects of a farm of flap-type devices without optimizing the power production. A similar numerical approach was used by [24] to study the power production and layout optimization of different farm configurations of flap-type devices. Different control techniques are used by [25–27] to combine optimal array layout design and optimal control performance. Although a co-design approach is implemented, it is focused on energy maximization or cost reduction, and the assessment of coastal protection is never considered.

Different types of WEC are present in the literature of coastal protection applications of WEC farms. [28] presents both experimental and numerical results for a floating attenuator with a hinged horizontal flap: several wave and installation conditions are investigated, but the properties of the system are kept constant and are not considered as control variable. [29] evaluates the field effects of a farm of both heaving point absorbers and oscillating surge WECs while varying the Power Take-Off (PTO) model; however, no optimization is pursued. A floating overtopping WEC is tested, in two different geometries, in a laboratory tank to investigate coastal protection performance against flooding [30]. The influence of sea level rise on the performance of a dual wave farm is tackled in [31], combining a spectral wave propagation model and a sediment transport formulation. In [32], an Artificial Neural Network is developed for the assessment of the efficiency of a WEC farm for coastal protection. All these studies, however, focus on the effect of the presence of a farm on the nearby shore, never considering the possible energy extraction.

To the best of authors' knowledge, the body of literature in wave energy conversion considers *either* one of the two aspects:

(i) control and layout optimization, without considering the total wave field attenuation within the objective function, or
(ii) quantification of the wave attenuation of a given WEC farm, without tuning the PTO or modifying the layout with the explicit purpose to maximize coastal protection.

While a preliminary exploration of concurrent power extraction and wave attenuation is conducted in [33] for a small floating WEC farm, it is noteworthy that comprehensive research on this topic is notably lacking in the existing literature. However, in principle, it can be reasonably expected that varying the control action to optimize power extraction will also modify the wave attenuation field. Therefore, the novelty of this paper is to argue that both productivity and wave attenuation should be concurrently considered as eligible objective functions. The interplay between these objectives is quantitatively explored to assess their degree of equivalence. Specifically, the study aims to determine whether optimizing for the highest power extraction automatically leads to maximizing coastal protection, and vice versa. If there is a strong correlation between the respective optima, it implies that these optimization objectives are interchangeable and equivalent. However, if there are significant differences between the optimum solutions, it becomes crucial to make a conscious engineering choice regarding their priority.

Regarding layout optimization, this trade-off becomes a static decision that cannot be modified once implemented. In contrast, the tuning of the control strategy offers more flexibility, as it can be dynamically adjusted online. Consequently, it becomes possible to vary the compromise between power extraction and coastal protection based on factors such as sea state, period of the year (considering other uses of the sea in maritime spatial planning), coastal conditions, or the condition of the WEC itself. This dynamic control strategy allows for adaptable and context-specific optimization based on real-time considerations.

In summary, the purpose and novelty of this paper is to quantitatively elaborate on the interplay between the two beneficial uses of WECs described above, namely clean energy production and coastal protection. Additionally, it delves into multi-objective optimization by creating a Pareto front through an exhaustive search for control parameters. Two different WECs have been firstly considered (a floating pitching WEC and an oscillating surging WEC), since the significance of wave attenuation capability with respect to power production depends on both hydrodynamic characteristics and the working principle of the WEC. However, the focus of this paper is not an exhaustive treatment of design choices for different classes of WECs, nor layout optimization,

but rather the study of the influence that tuning PTO parameters has on both power production and the resulting perturbed wave field.

The reminder of the paper is as follows. Section 2 describes the numerical model, based on linear potential flow implemented via boundary element method, while Section 3 presents and compares the characteristics of the two WECs herein considered. Consequently, the influence of the control strategy is thoroughly analyzed in Section 4, for a single device. In Section 5 the farms of three and five OSWCs are investigated. Finally, Section 6 presents some final remarks and conclusions.

2. Numerical model

This study employs the BEM (Boundary Element Method), a potential flow theory-based approach, in which the fluid is assumed to be inviscid and incompressible, and the flow irrotational.

Thus, defining the spatial variable $\mathbf{x} = (x, y, z)$, and the temporal variable t, there exists a velocity potential $\Phi(\mathbf{x}, t) = \mathrm{Re}[\phi(\mathbf{x})\, e^{i\omega t}]$, satisfying Laplace's equation $\nabla^2\phi = 0$ in the entire domain, with ω the angular wave frequency.

Considering small amplitude motions of a body in the domain, and small wave amplitude, a linearity assumption is justified. Consequently, the free surface, defined as:

$$\eta = -i\frac{\omega}{g}\phi|_{z=0}, \tag{1}$$

with gravity g, depends on the total perturbed potential ϕ^P:

$$\phi^P = \phi^I + \phi^D + i\omega \sum_{\delta=1}^{N_{DOF}} \zeta_\delta \phi_\delta^R. \tag{2}$$

The perturbed potential of a unit amplitude wave, is the superposition of three elements: the incident ϕ^I, radiated ϕ^R, and diffracted ϕ^D potentials. The radiated potential is further related to the body's motions – the N_{DOF} Degrees of Freedom (DoFs) – through the Response Amplitude Operator (RAO) of the δ-th degree of freedom.

A boundary value problem is defined, and is solved with the BEM solver Capytaine [34], the Python implementation of NEMOH, developed at Ecole Centrale de Nantes, France [35].

For the analysis of the power extraction, the WEC is equipped with a PTO system, which typically exhibits complex nonlinear behavior [36] due to the implementation of sophisticated control strategies to maximize power output [37]. However, for frequency domain analysis it is often acceptable to linearize the PTO [38], so that the superposition principle holds, allowing for simplification as a spring–damper system. The equation of motion [39] for the displacement $\zeta(\omega)$, implementing the PTO model, is:

$$[-\omega^2(\mathrm{M} + \mathrm{A}) + i\omega(\mathrm{B} + \mathrm{B}_{PTO}) + (\mathrm{C} + \mathrm{C}_{PTO})]\zeta = \mathrm{F}, \tag{3}$$

where M is the body mass matrix, A denotes the added mass matrix, B the radiation damping matrix, C the matrix of hydrostatic and gravitational restoring coefficients, and F represents the external excitation forces, defined as the sum of diffraction and Froude–Krylov forces [40]. The matrices B_{PTO} and C_{PTO}, are, respectively, the damping and stiffness associated to the linear PTO.

The mean power absorbed by a WEC over a monochromatic wave period is

$$P = \frac{1}{2}\omega^2 \zeta^T \mathrm{B}_{PTO} \zeta^*, \tag{4}$$

using the superscripts ^{T} to represent the transpose and * the complex conjugate.

In this study, a linear PTO model is used to simulate the behavior of the PTO system, and two typical control strategies used for WECs are considered, both with constant coefficients: reactive control and passive control. In the passive control strategy, the PTO system is configured to provide only a linear PTO resistance load (damping force). On the other hand, in the linear reactive control strategy, both the PTO reactance and the PTO damping coefficient can be varied to tune the device's behavior. By adjusting these parameters, the WEC's response can be optimized to achieve maximum power absorption. For WECs with one DoF under passive control, the power absorption is maximized when

Passive PTO	Reactive PTO
$B^p_{PTO} = \sqrt{B^2 + \frac{1}{\omega^2}\left(-(M+A)\omega^2 + C\right)^2}$	$B^a_{PTO} = B$
$C^p_{PTO} = 0$	$C^a_{PTO} = (M+A)\omega^2 - C$

(5)

It is worth noting that such conditions for maximum power extraction are valid for a linear unconstrained monochromatic system, while sub-optimal otherwise. However, this is not a limitation for the current study, since the focus is to investigate the interplay between power absorption and wave attenuation. In order to draw meaningful conclusions, it is sufficient to have a level playing field of comparison; in addition, it is preferable to maintain simple simulating conditions (i.e. linear unconstrained model), to make results intelligible and facilitate interpretation via inference of causality.

To investigate the sensitivity of the control strategies on WEC performance, either in power extraction and wave field attenuation, we vary the values of B_{PTO} and C_{PTO} to tune the system's response. We then compare the results with an uncontrolled WEC configuration, where B_{PTO} and C_{PTO} are both set to zero. This uncontrolled scenario serves as a baseline for evaluating the effectiveness of the control strategies in enhancing power absorption and overall WEC performance.

For the analysis of the environmental impact, the disturbance coefficient K_d, defined as

$$K_d = \eta^P / \eta^I, \tag{6}$$

is used, where η^P is the total perturbed free surface elevation amplitude, whereas η^I is the undisturbed one; therefore, the disturbance coefficient represents the change in the wave field caused by the presence and action of the body with respect to the condition with only an incident wave. In particular, within a coastal protection perspective, the interest is in minimizing K_d, so as to reduce the impact of the wave field especially in the lee of the body.

In this study, the simulation domain for the BEM is a 800 m × 800 m grid, with uniform spatial discretization of 2 m in both directions. The single WEC and the farm of WECs are all placed in the center of the domain, placing the shoreline at a distance of 400 m, or less. This distance aligns with the requirements for coastal protection and the shallow water depth requirement for the OSWC technology. Higher fidelity models might offer greater accuracy but come at the cost of significantly higher computational resources. On the other hand, the BEM, despite being less precise, especially in power estimation [41], remains computationally manageable.

The linear potential theory used in this study prevents the simulation of extreme events. Typically, WEC designs incorporate mechanisms to handle such scenarios, including transitioning into survival mode. For instance, certain WECs may cease the PTO and energy extraction, but their physical presence can still generate a wake, leading to wave attenuation. However, this study does not cover such cases.

Moreover, the distance of the WEC or WEC farm from the shore also endorses the representation of the waves as planar: assuming a coast developing for several meters, the approaching waves tend to become normal to the shore as they propagate towards shallow waters [42]. Furthermore, to appropriately address the conditions of a particular sea site, high-quality metocean data would be essential, as highlighted in [43]. However, for the purpose of simplicity and broad applicability, this study opts for regular waves.

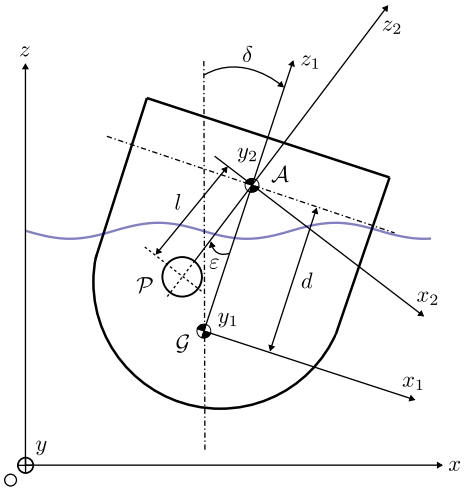

Definition	Value
Hull length	14.8 m
Hull width	22.5 m
Hull height	7.4 m
Hull draft	4.81 m
Hull mass	1118 t
Moment of inertia	2.99×10^7 kg m^2
Resonance frequency	0.96 rad/s

Fig. 1. PeWEC's schematic design and main technical characteristics, inspired by [44].

3. Comparative analysis of PeWEC and OSWC

In this section, we compare two different WECs, based on distinct working principles, the PeWEC (Pendulum Wave Energy Converter) and the OSWC (Oscillating Surge Wave Converter). The PeWEC is designed for closed seas and operates as a rotating mass device, extracting energy through the pitching motion of a floating hull. It utilizes a pendulum's relative motion to the shaft of an electrical generator for power extraction [44]. As a directional device, PeWEC aligns with the incoming waves thanks to a mooring system based on a spreading catenary. The OSWC is a pitching flap, hinged at its base to a fixed axis, secured to the seabed, and primarily operates in shallow to intermediate waters [45]. The oscillatory movement of the OWSC drives two hydraulic cylinders connected to the flap and the fixed sub-frame, generating electricity through an electrical generator placed onshore. The OSWC is also a directional device, and works at its best with incoming waves without spreading.

A sketch of the devices and their technical features are displayed in Figs. 1 and 2, for the PeWEC and OSWC, respectively.

A comparison of the hydrodynamics of both WECs (see Fig. 3) reveals different behaviors. Despite different orders of magnitude in absolute value, the trend of the radiation damping is similar for the two devices. The diffraction force, however, shows a very different behavior, with a single peak for the OSWC compared to the configuration of peaks and throats of the PeWEC. Radiation and diffraction forces, along with the hydrostatic stiffness and inertial properties, contribute to build up the RAO which, in turns, determines the amplitude of the response and the power extraction.

The wave field attenuation depends on both the radiation and diffraction contributions. On the one hand, the effect of diffraction is independent from the motion response, at least in the linear approximation, and mostly depends on the geometric characteristics: the OSWC device is much taller than the PeWEC, and so its encumbrance; hence the magnitude of diffraction is larger, and only one peak period is present. Conversely, the PeWEC is a floating device, hence diffraction is smaller, and with multiple peaks. On the other hand, the effect of radiation depends also on the amplitude of the response, since the radiation force is obtained multiplying the radiation damping and the velocity. Therefore, while both radiation and diffraction depend on the wave period, it can be expected that PTO tuning affects only the component of wave attenuation due to radiation.

Finally, although Fig. 3 clearly shows a different hydrodynamics for the two WEC types, it is not sufficient to conclude on their effectiveness as wave attenuators. For this reason, a visualization of the wave fields is shown in Fig. 4, in terms of disturbance coefficient K_d. In particular, the top row of Fig. 4 is obtained by summing to the unperturbed wave field, the radiation and diffraction perturbations, that are displayed separately. Note that, in order to simplify the graphical representation with the same color bar scale, radiation and diffraction contributions are presented in absolute values, instead of negative and positive.

Both WECs are analyzed at their respective resonance period, where their motion and power extraction is most significant. The radiating component of K_d reflects the behavior of the radiation damping seen in Fig. 3, showing similarities for both the OSWC and the PeWEC. In contrast, the diffraction pattern is distinctly circular for the PeWEC, and the values smaller. The OSWC, having a similar shape for both the radiating and diffracting contributions, presents an oscillatory perturbed wave field in front of the device and a visible wake downstream. Conversely, the PeWEC produces a zone of increased wave height in its lee, going against the principle of wave attenuation we are seeking in this study.

Therefore, Fig. 4 suggests that the PeWEC is not as effective for coastal protection as the OSWC. Similar conclusions can be obtained for other wave frequencies, which have not been presented here for compactness.

Nevertheless, considering that a WEC intended for both wave attenuation and power extraction would invariably feature a PTO system, the forthcoming section provides an overview of the implementation of two control strategies before making definitive comparisons between the OSWC and the PeWEC.

4. Influence of the control strategy on a single device

The incorporation of a PTO system in WECs enables the conversion of mechanical energy into electricity, resulting in power production. Simultaneously, the presence of the PTO system alters the motion response of the WEC body, leading to notable effects on the surrounding wave field, particularly the radiated wave field, which is directly linked to the RAO of the WEC (see Eq. (2)). Considering the complexity of control strategies and their potential impact on WEC performance, a preliminary analysis using a linear PTO model is implemented (see Eq. (3)) with two strategies: passive and reactive PTO. By initially using

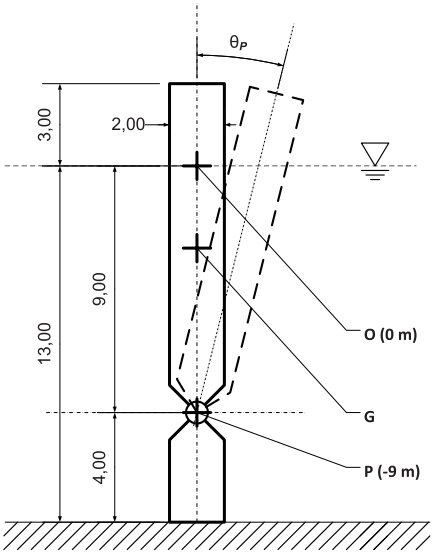

Definition	Value
Flap width	26 m
Flap thickness	2 m
Flap height	12 m
Flap freeboard	3 m
Flap mass	150 t
Moment of inertia	8.12×10^6 kg m^2
Resonance frequency	0.36 rad/s

Fig. 2. OSWC's schematic design and main technical characteristics, inspired from [45].

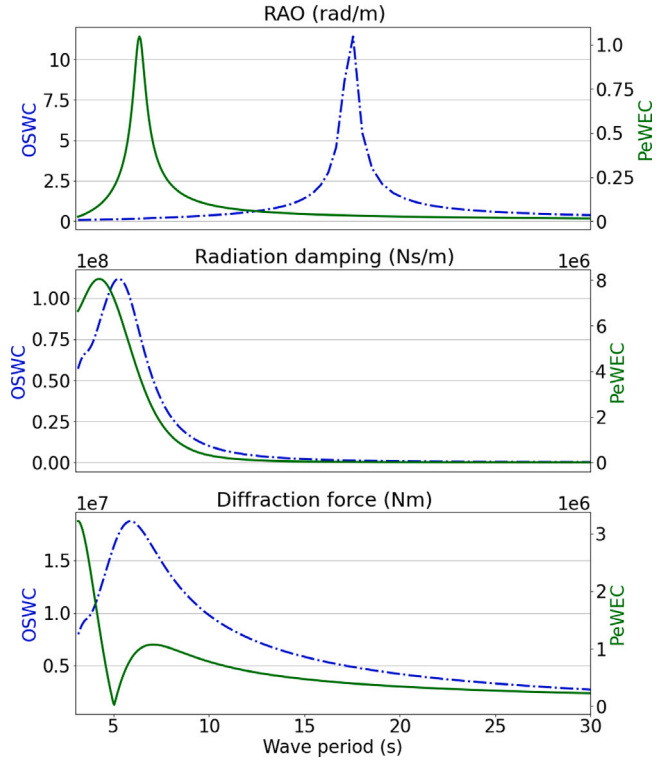

Fig. 3. Evolution of the RAO, the radiation damping and magnitude of diffraction force coefficient with the wave period, for the OSWC and the PeWEC.

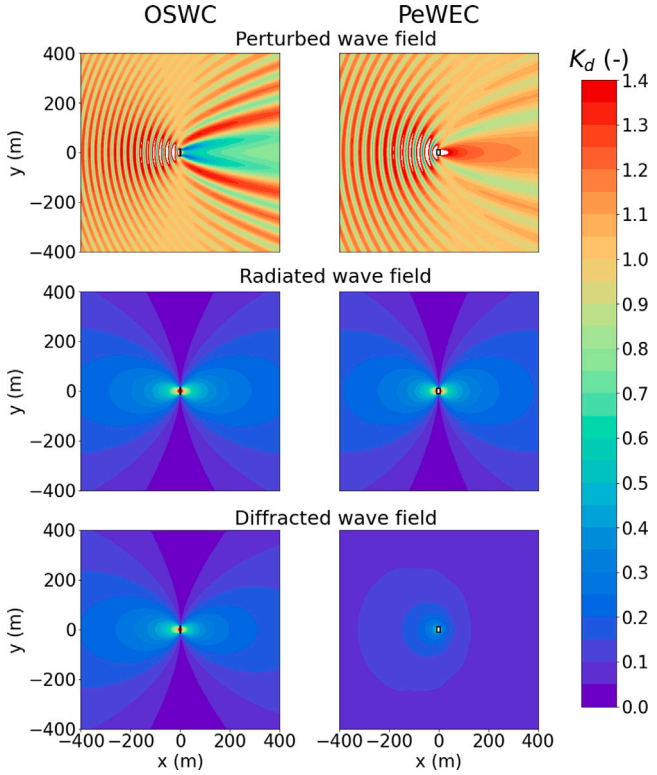

Fig. 4. Overview of the perturbed, radiated and diffracted wave fields, in terms of disturbance coefficient, for the OSWC and the PeWEC, at their respective resonance period. Note that radiation and diffraction perturbations are plotted in absolute values.

optimal values for B_{PTO} and C_{PTO}, the corresponding free surface is calculated, along with the size of the wake behind the WEC, when present. The wake is identified as the continuous region for which there is a wave attenuation of at least 10% (so K_d <= 0.9); in this definition, *continuous* refers to the fact that nowhere within the region K_d is allowed to be above 0.9. Such a limit of 0.9 is a reasonable threshold to consider that a WEC farm is bringing a beneficial wave attenuation effect and an effective coastal protection. In addition to the wake width, a wake intensity, drawing inspiration from the Betz limit in the wind energy sector, is defined as the area included below the K_d <= 0.9 (the colored zone in Fig. 5(b)), relative to the area of the same extension from the line at $K_d = 0.9$ to $K_d = 0.0$ (no wave).

Within the wake region, different sections can be taken at different distances in the lee of the WEC, effectively representing different relative position between the WEC and coastline; in this way, it is possible to elaborate on the most convenient installation distance from shore of a potential farm in order to obtain the required coastal protection

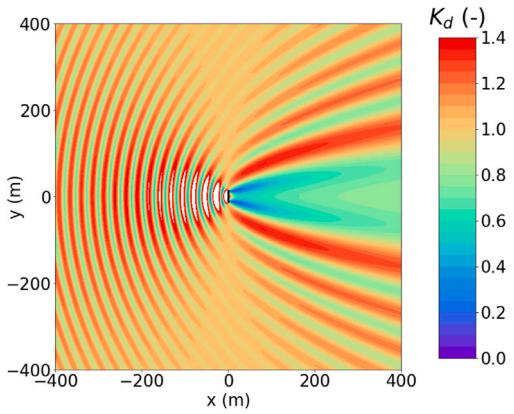

(a) K_d over the entire domain. The blank values are outside the range of the colorbar.

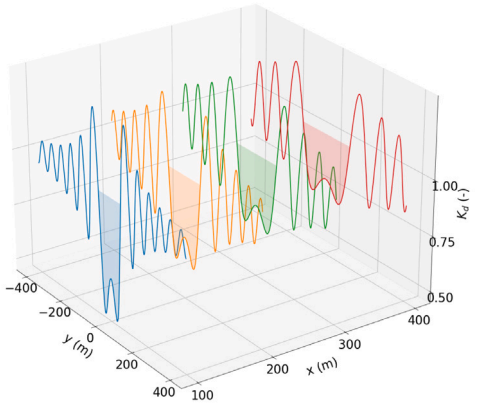

(b) y-sections at $x = 100, 200, 300, 400$ m behind the WEC. The shaded area is for $K_d <= 0.9$ and allows to identify the wake.

Fig. 5. Free surface, in terms of disturbance coefficient, for the single OSWC, without PTO, at $T = 6$ s.

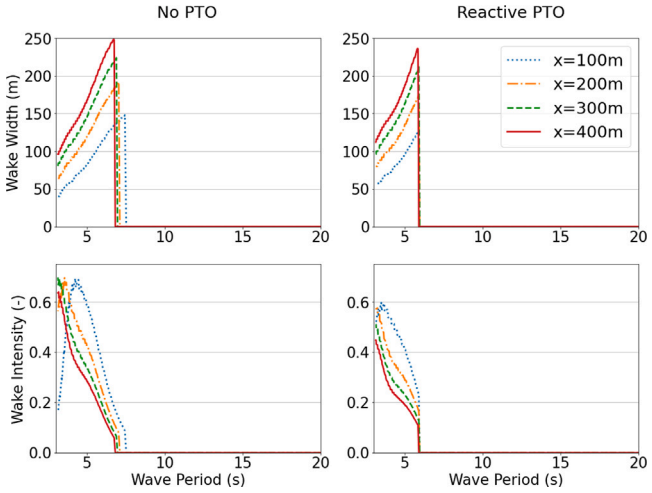

Fig. 6. Evolution of the wake, in terms of width and intensity, of the OSWC with the wave period, for the single WEC, without PTO, and with reactive PTO.

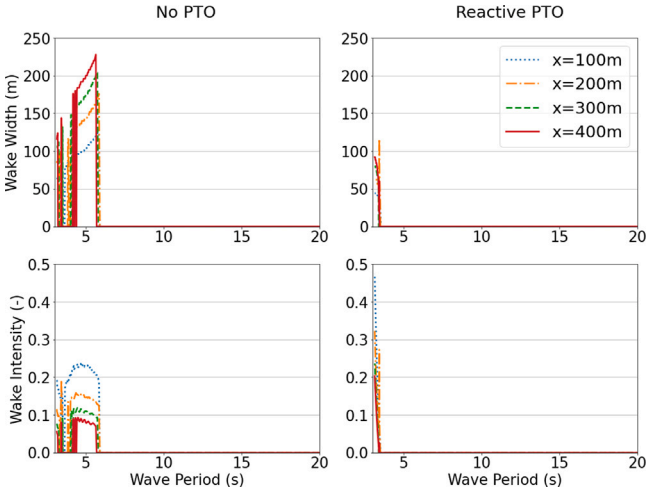

Fig. 7. Evolution of the wake, in terms of width and intensity, of the PeWEC with the wave period, for the single PeWEC, without PTO, and with reactive PTO.

objectives. The section at the domain limit, i.e. at $x = 400$ m, is chosen as the nominal distance for the comparison along the entire paper. In Fig. 5, a visual representation of the wake is shown, showing multiple y-sections. As Fig. 5(a) shows, the OSWC gives an oscillating perturbed wave field in the front part of the WEC, but also creates a wake in its lee. The wake width increases with increasing distance from the WEC. However, the wake intensity decreases, since the wake is less and less deep. In the case displayed in Fig. 5(b), the wake width goes from 116 m at $x = 100$ m to 220 m at $x = 400$ m, and the wake intensity goes from 0.34 to 0.15. The wake width and intensity are then computed for the entire range of wave periods considered, and the results are shown in Fig. 6.

Reactive control, with its two adjustable parameters, offers the most favorable conditions for optimizing power extraction, representing the optimal scenario in this regard. Conversely, passive control generally results in reduced power production compared to reactive control. When examining the wave attenuation behind the WEC, as depicted in Fig. 6, we observe two cases: one without PTO (and consequently, no power production), and another with reactive PTO, known for its superior power production performance. Since the passive control case yields wake results similar to reactive control, it is not shown. In both scenarios, a wake is observed, but only for a limited range of wave periods. Specifically, the wake widens as the wave period increases until approximately $T = 7$ s, beyond which it vanishes for longer periods. Interestingly, the intensity of the wake follows an opposite trend, indicating that for longer wave periods, the wake becomes broader but less intense. The presence of PTO appears to eliminate the wake after around $T = 6$ s, so at smaller periods compared to the case without control. This observation suggests that for larger wave periods, particularly near the WEC's resonance, the device experiences substantial excitation, resulting in a pronounced radiation effect compared to diffraction. Consequently, the surrounding wave field is significantly disturbed and not attenuated. Moreover, when the PTO is present, the wake is slightly smaller and less intense than the case of the uncontrolled WEC.

Although the differences in the wake of the two cases (no PTO and reactive PTO) seem negligible, they are an indicator that modifying the PTO tuning parameters has an impact on the wave attenuation pattern, already with the single device. However, using optimal PTO

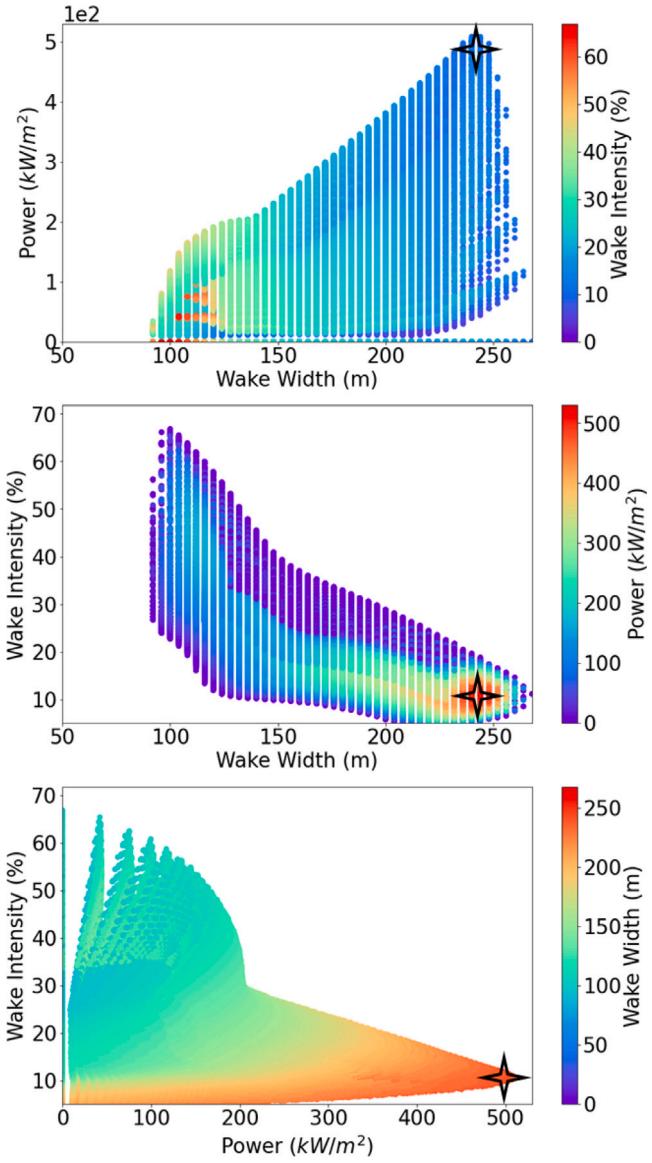

Fig. 8. Representation of the variable PTO analysis, varying the point cloud according to power, wake width and wake intensity. The points represent all the combinations of B_{PTO}, C_{PTO}, and wave period, for the single OSWC case. The color represents the value, according to the respective color bars. The star represents the area of maximum possible power.

parameters alone might not lead to substantial wave attenuation. It is worth noting that such small periods are typical of closed seas, like the Mediterranean Sea, where the OSWC would not produce at its potential maximum, but would have a dual positive effect on the coast.

When examining the PeWEC without the PTO system, we observe that the wake width is comparable to that of the OSWC. However, it is accompanied by instabilities and notably reduced wake intensity, as illustrated in Fig. 7. Upon implementing the PTO system for the PeWEC, the results exhibit a stark contrast, with the wake disappearing rapidly for smaller wave periods. This behavior can be attributed to the fact that at $T = 6\,\mathrm{s}$, the wave period is in close proximity to the resonance of the PeWEC. During resonance conditions, the PeWEC experiences maximum excitation and may not generate a wake, similar to the OSWC. Additionally, being a floating device, it generates minimal diffraction. These observations, along with the insights discussed in Section 3, collectively strengthen the conclusion that the PeWEC's effectiveness in terms of coastal protection is limited. Nonetheless, the PeWEC could be considered a more versatile option for installation in comparison to the OSWC. While its wave attenuation capabilities may be modest, they may still be adequate to meet specific requirements at certain sea sites, which may impose less stringent wave attenuation criteria than the 10% chosen for this study. However, for the sake of simplicity, the remainder of the paper focuses on the OSWC.

To gain further insights into the variability of the two objectives of the study, a PTO with variable values for damping and stiffness is implemented for the OSWC. Therefore, B_{PTO} is varied in a uniform way in the range $\{0, 2e8\}$Nms, and C_{PTO} in the range $\{-2e8, 2e8\}$Nm for the whole range of wave periods considered. Such analysis, based on the exhaustive search method, allows to consider the impact of the PTO on wave field attenuation, when the primary focus is not solely on maximizing power production.

Given that the parameters of interest are power, wake width, and wake intensity, they are visualized on distinct two-dimensional Pareto fronts, as shown in Fig. 8, to have an insights into their trade-offs. Notably, only a limited set of combinations of B_{PTO}, C_{PTO}, and wave period can simultaneously achieve high power and a broad wake, as indicated by the star on the plots. While these combinations result in a relatively shallow wake, they guarantee at least 10% wave attenuation. However, if a more substantial wave attenuation is required, a compromise between extended attenuation and power output must be sought. Furthermore, when the wave period is fixed at $T = 6\,\mathrm{s}$, where the presence of a wake is established from previous results, Fig. 9 illustrates how wake characteristics and power vary with different PTO values. It becomes evident that optimizing the PTO for maximum wave attenuation does not align with the goal of maximizing power extraction. The peak wake, in terms of width or intensity, is achieved with small values of B_{PTO}, which, in turn, yield low power output. Conversely, a trade-off appears more likely for positive stiffness values. In any case, the passive control strategy is not particularly advantageous (the horizontal line at $C_{PTO} = 0\,\mathrm{MNm}$).

The same analysis may be done for other distances of the coast from the WEC (see Fig. 5(b)) and find different combinations of the parameters. Furthermore, this result is valid for a single device: considering multiple WECs in farms may alter the observed behavior. In fact, all of the above considerations have served the purpose to build up sensitivity about the effect of each parameter on the overall behavior; more meaningful considerations, closer to a more realistic array application case, as presented in Section 5.

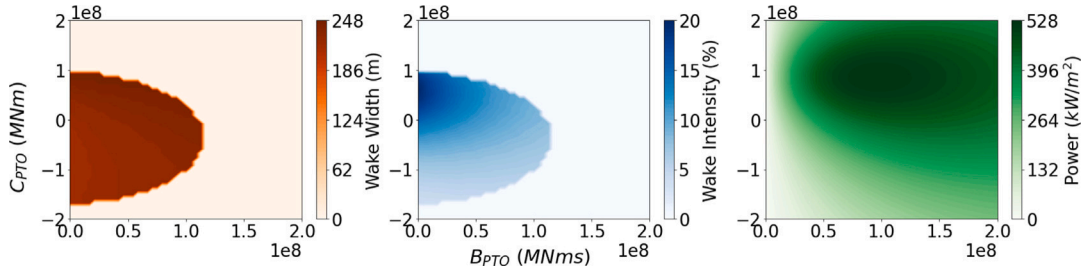

Fig. 9. Representation of the variable PTO analysis, for the single OSWC at $T = 6\,\mathrm{s}$. The parameters of interest (wake width, wake intensity, and power) are displayed with different colors, for varying values of B_{PTO} and C_{PTO}.

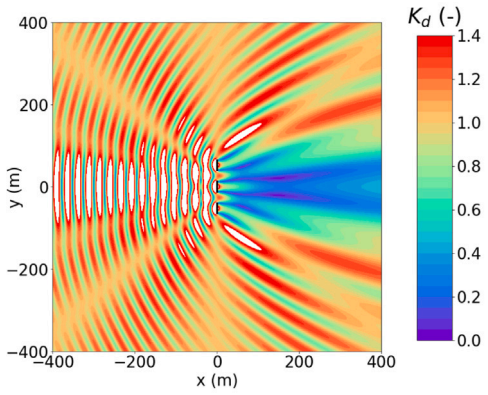

(a) K_d over the entire domain. The blank values are outside the range of the colorbar.

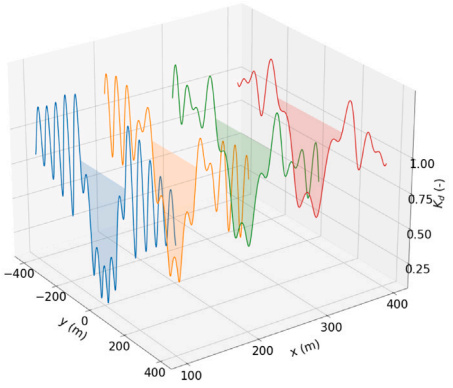

(b) y-sections at $x = 100, 200, 300, 400$ m behind the farm. The shaded area is for $K_d <= 0.9$ and allows to identify the wake.

Fig. 10. Free surface, in terms of disturbance coefficient, for the 3-WEC aligned farm, without PTO, at $T = 6$ s.

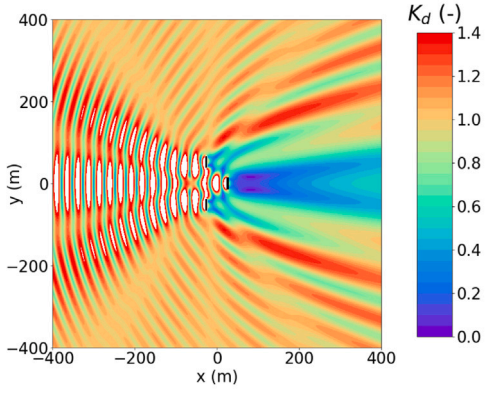

(a) K_d over the entire domain. The blank values are outside the range of the colorbar.

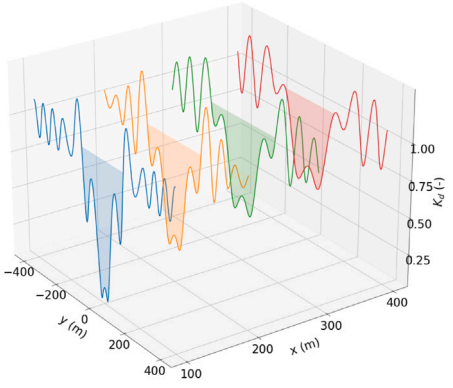

(b) y-sections at $x = 100, 200, 300, 400$ m behind the farm. The shaded area is for $K_d <= 0.9$ and allows to identify the wake.

Fig. 11. Free surface, in terms of disturbance coefficient, for the 3-WEC staggered farm, without PTO, at $T = 6$ s.

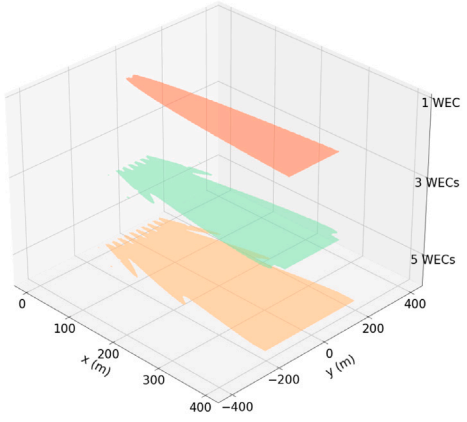

(a) Aligned layout.

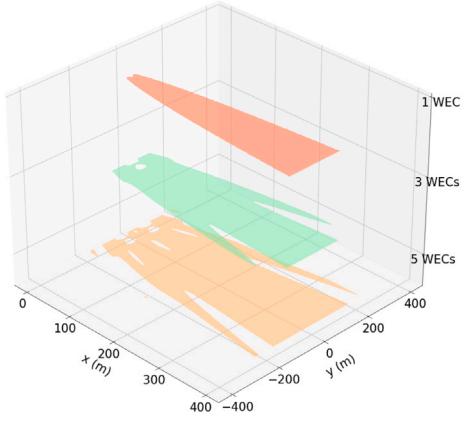

(b) Staggered layout.

Fig. 12. Wake behind the single WEC and the farm of 3 and 5 WECs, for the different layouts. $T = 6$ s and there is no PTO.

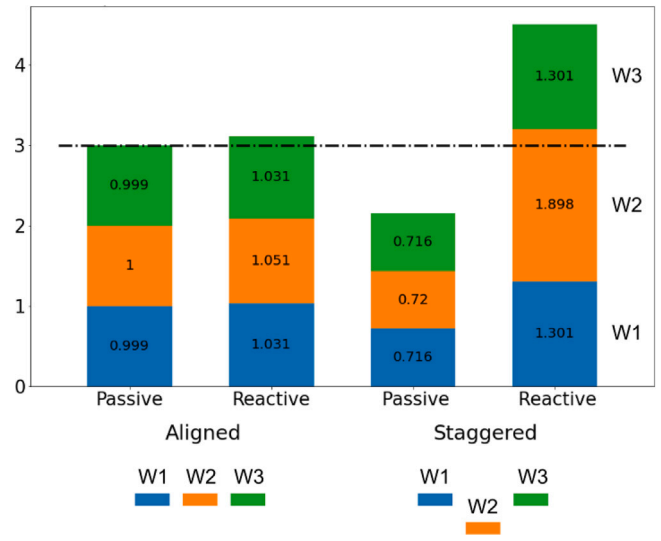

Fig. 13. The q-factor for each WEC in the 3-WEC farms, both aligned and staggered configurations, is graphically represented here. In this context, the q-factor is defined as the ratio of the power produced by an individual WEC within the farm to the power generated by a standalone WEC employing the same control strategy. The black line in the graph represents the threshold for 3 isolated devices. When the q-factor is below this threshold, it indicates that the farm's overall power extraction is less efficient. Conversely, when the q-factor exceeds this threshold, grouping the OSWCs closely together results in more favorable outcomes.

5. Influence of the control strategy on WEC farms

WEC farms offer various deployment possibilities, including different layouts and distances between devices, presenting a multitude of potential scenarios. Considering the proximity of these farms to the coast and installation constraints, this study focuses on farms consisting of one or two lines of WECs. Moreover, the number of WECs is limited to three or five, as they create an array that can be seen as modular, replicable several times for larger installations. As for the distance among the WECs, it has to be large enough for maintenance and cabling cost purposes; however, if it is too large, no interactions occur and each WEC can be considered as a single device. For all these reasons, two sets of farm layouts are analyzed: an aligned farm, a staggered farm, each counting 3 or 5 WECs. The inter-device distance is twice the WEC length in both directions. Although interactions are dependent on the WEC spacing, we limit ourselves to a unique distance, in order to focus on the effect of the tuning of the PTO; nevertheless, the distance chosen is typically representative of the optimal spacing found in optimization studies in the literature [25,46]. Each WEC in the farm is equipped with passive or reactive PTO systems, with the optimal values for B_{PTO} and C_{PTO} that, in principle, may be different for all of them. While in practical applications, it is preferable for each device within the farm to have its individualized and ideally tuned PTO system, and more efficient control strategies may be available, this study opts for a uniform PTO configuration across all WECs within the farm, consistent with that of the single device. In the scenarios involving the use of optimal values, as specified by Eq. (5) using matrices, the interactions among WECs are factored into the PTO system. When investigating the variable PTO values, all WECs within the farm are assigned the same parameter value. This approach, although potentially suboptimal in terms of control, is chosen to maintain simplicity in the analysis.

In addition to the classical power (Eq. (4)), the q-factor is used, representing the power extracted by the farm compared to the power extracted by the same number of devices considered separately, and is defined as:

$$q = \frac{P_a}{n_B\, P_s}, \tag{7}$$

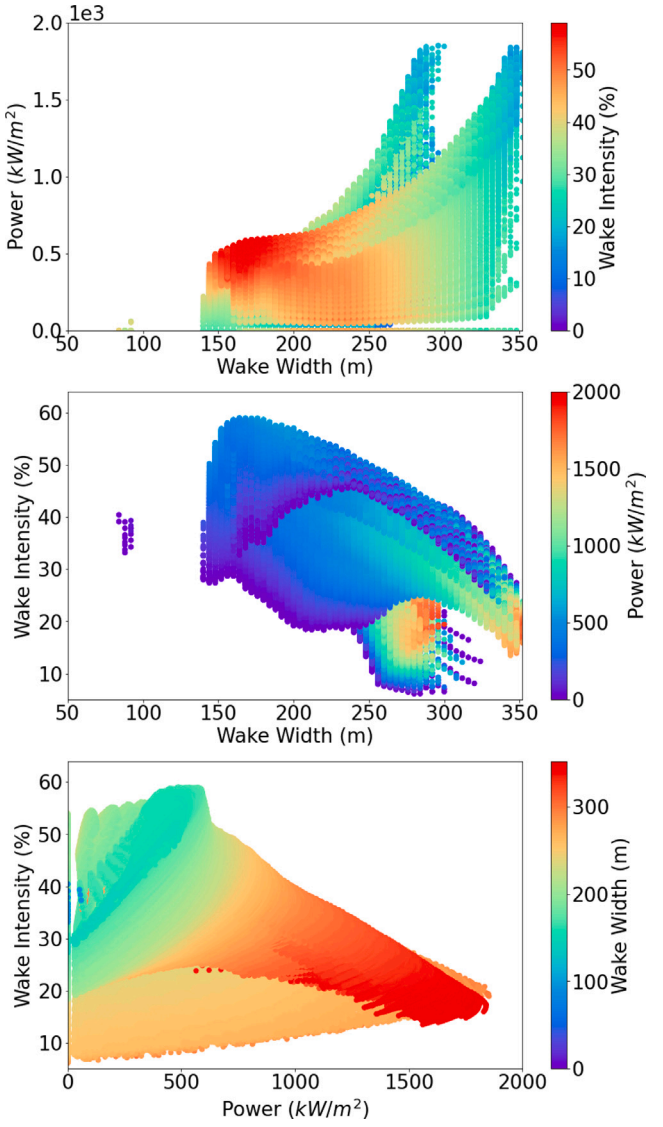

Fig. 14. Representation of the variable PTO analysis, varying the point cloud according to power, wake width and wake intensity. The points represent all the combinations of B_{PTO}, C_{PTO}, and wave period, for the 3-WEC aligned farm case. The color represents the value, according to the respective color bars.

where P_a is the power extracted by the farm, P_s the power extracted by the single device in the same conditions, times the number of bodies n_B. A value of q above unity indicates positive interactions leading to increased power production; conversely, if $q < 1$, putting the WECs in a farm is not convenient, as the overall power decreases.

In the aligned farm layout, 3 or 5 WECs are placed on a single line, all of them exposed to the incoming waves, see Fig. 10. The WEC in the middle is influenced in a symmetrical way by the WECs on the sides, resulting in a stronger impact on the wave field compared to a single WEC (Fig. 12(a)). In the staggered farm configuration, one, and two WECs are positioned behind the first line, which partially covers them from the incoming waves. The resulting wave field is also symmetrical (Fig. 11), and the interactions are strong, since the WECs are closer together with respect to the aligned layout. From Figs. 10, 11, 12, the different wake, especially close to the WEC farm is clear. At $x = 400$ m, the wake of the aligned farm is slightly larger and more uniform than the staggered farm one, but both are larger than the wake of a single OSWC, motivating the need for deploying multiple WECs together to increase wave attenuation, and not only power production.

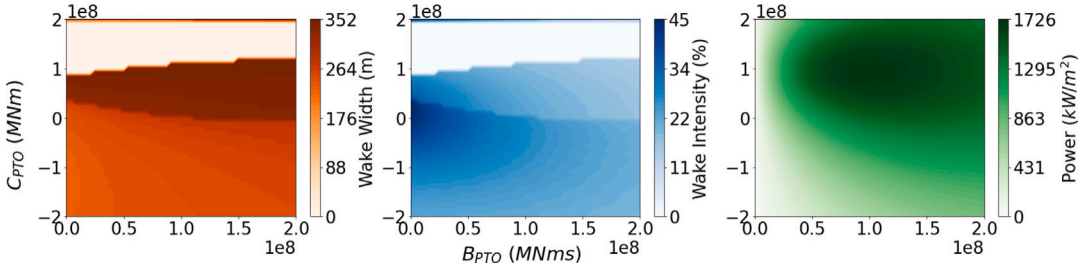

Fig. 15. Representation of the variable PTO analysis for the 3-WEC aligned farm, at $T = 6$ s. The parameters of interest (wake width, wake intensity, and power) are displayed with different colors, for varying values of B_{PTO} and C_{PTO}.

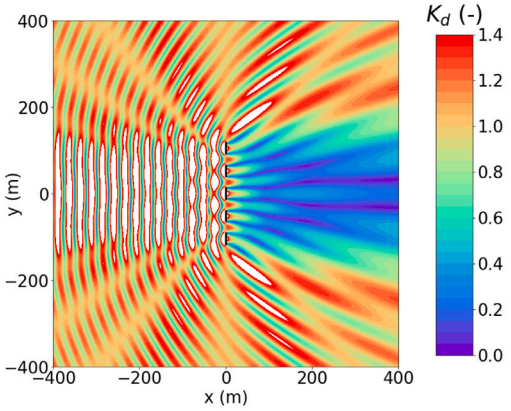

(a) K_d over the entire domain. The blank values are outside the range of the colorbar.

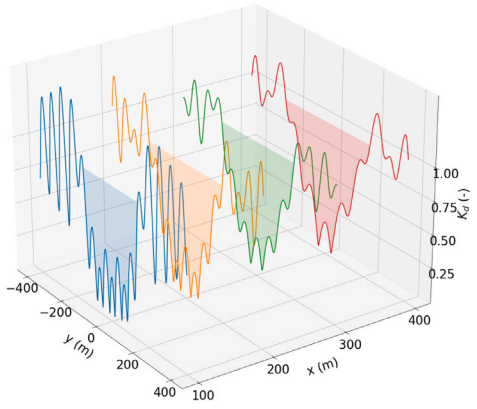

(b) y-sections at $x = 100, 200, 300, 400$ m behind the farm. The shaded area is for $K_d <= 0.9$ and allows to identify the wake.

Fig. A.16. Free surface, in terms of disturbance coefficient, for the 5-WEC aligned farm, without PTO, at $T = 6$ s.

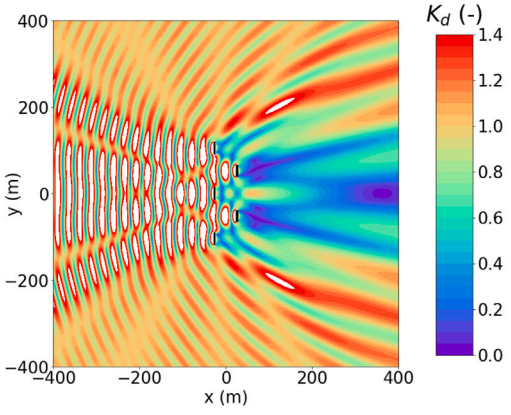

(a) K_d over the entire domain. The blank values are outside the range of the colorbar.

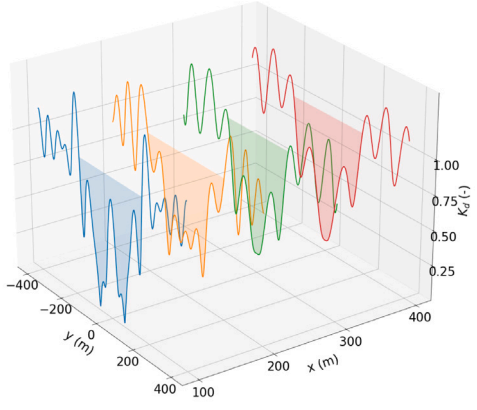

(b) y-sections at $x = 100, 200, 300, 400$ m behind the farm. The shaded area is for $K_d <= 0.9$ and allows to identify the wake.

Fig. A.17. Free surface, in terms of disturbance coefficient, for the 5-WEC staggered farm, without PTO, at $T = 6$ s.

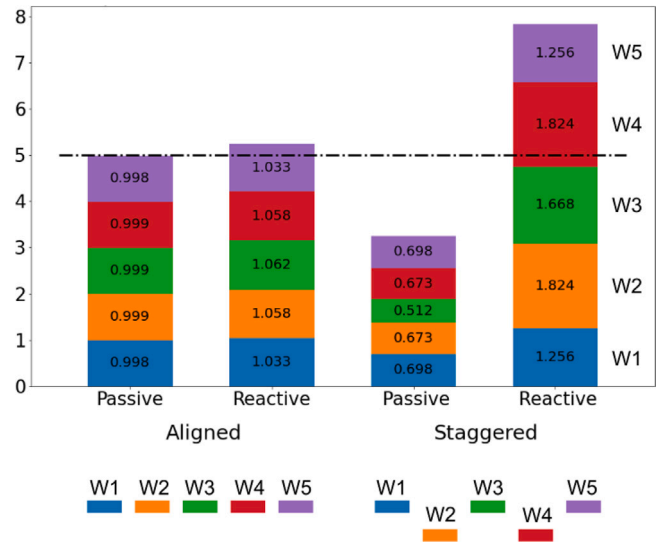

Fig. A.18. The q-factor for each WEC in the 5-WEC farms, both aligned and staggered configurations, is graphically represented here. In this context, the q-factor is defined as the ratio of the power produced by an individual WEC within the farm to the power generated by a standalone WEC employing the same control strategy. The black line in the graph represents the threshold for 5 isolated devices. When the q-factor is below this threshold, it indicates that the farm's overall power extraction is less efficient. Conversely, when the q-factor exceeds this threshold, grouping the OSWCs closely together results in more favorable outcomes.

Implementing the PTO in the model allows to extract energy and to further change the wake behind the farm. Computing the q-factor for each WEC in the farm, (Fig. 13), we can appreciate that a staggered WEC farm implementing reactive control is the most efficient in terms of power production, for $T = 6$ s. However, that configuration may not be the most effective in attenuate the wave behind the farm. Similar considerations can be made for the 5-WEC farms (see Appendix).

When the damping and stiffness values of the PTO are adjusted, an agreement between power production and wave attenuation becomes possible, even in the context of a WEC farm. In the case of the 3-WEC aligned farm (please refer to Fig. 14), the results exhibit a more intricate relationship compared to the single OSWC, while still demonstrating a trade-off between power output and wake width. In addition, the range of wake intensity is notably broader with respect to Fig. 8. These findings suggest that the 3-WEC aligned farm is favorable concerning all three parameters examined when compared to the isolated WEC case. Similar observations can be made for the 3-WEC staggered farm; however, the layouts of the 5-WEC farm lead to more complex plots (see Appendix). In this case, devising a control strategy to achieve an optimal trade-off becomes more intricate. Interestingly, at a wave period of $T = 6$ s, the plots for the WEC farms (Fig. 15) remain relatively consistent with those of the single WEC. This consistency implies that maximizing both power production and wave attenuation is not achievable with the same combination of B_{PTO} and C_{PTO}, highlighting the need for a compromise.

6. Conclusion

As the energy and environmental landscapes evolve, a comprehensive solution that harnesses wave energy for electricity generation while also mitigating wave forces reaching the shore to protect coastlines is essential. While it may be intuitive to assume that energy extraction from waves will result in an attenuated wave field near the coast, in reality, this may not always be the case. However, historically, power extraction and wave attenuation have been treated as separate considerations in the design of wave energy conversion technologies, leading to limited knowledge in this area. This paper takes a new

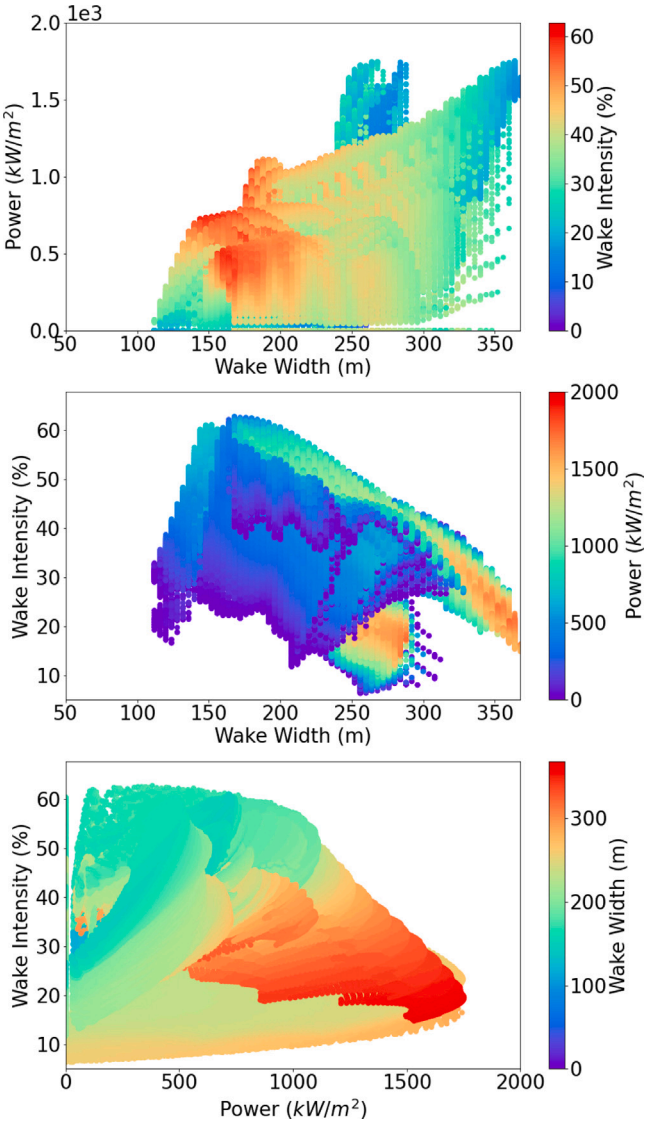

Fig. A.19. Representation of the variable PTO analysis, varying the point cloud according to power, wake width and wake intensity. The points represent all the combinations of B_{PTO}, C_{PTO}, and wave period, for the 3-WEC staggered farm case. The color represents the value, according to the respective color bars.

perspective with a holistic approach, considering multiple aspects of wave energy conversion technologies, which could have significant implications for marine sector strategies.

Initially, two different WEC technologies, PeWEC and OSWC, are analyzed. The hydrodynamics of these technologies are compared, both in their uncontrolled states and equipped with a linear PTO system, using passive and reactive control strategies. Given that the PeWEC demonstrates minimal wave attenuation, the focus of the study shifts towards the OSWC, which exhibits more potential for coastal protection purposes. Subsequently, a multi-objective optimization approach is employed, involving an exhaustive search of PTO parameters, particularly damping and stiffness, across various wave periods. This optimization strategy enables the integration of two initially separate objectives, power production and wave attenuation, yielding a Pareto front that showcases trade-offs between these two aspects. The results unveils a possible set of combinations of B_{PTO}, C_{PTO}, and wave period that can provide maximum power generation and wake width, albeit with a relatively mild wake intensity. Additionally, the presence of a wake is confined to wave periods up to $T = 6$ s, typically indicative of more

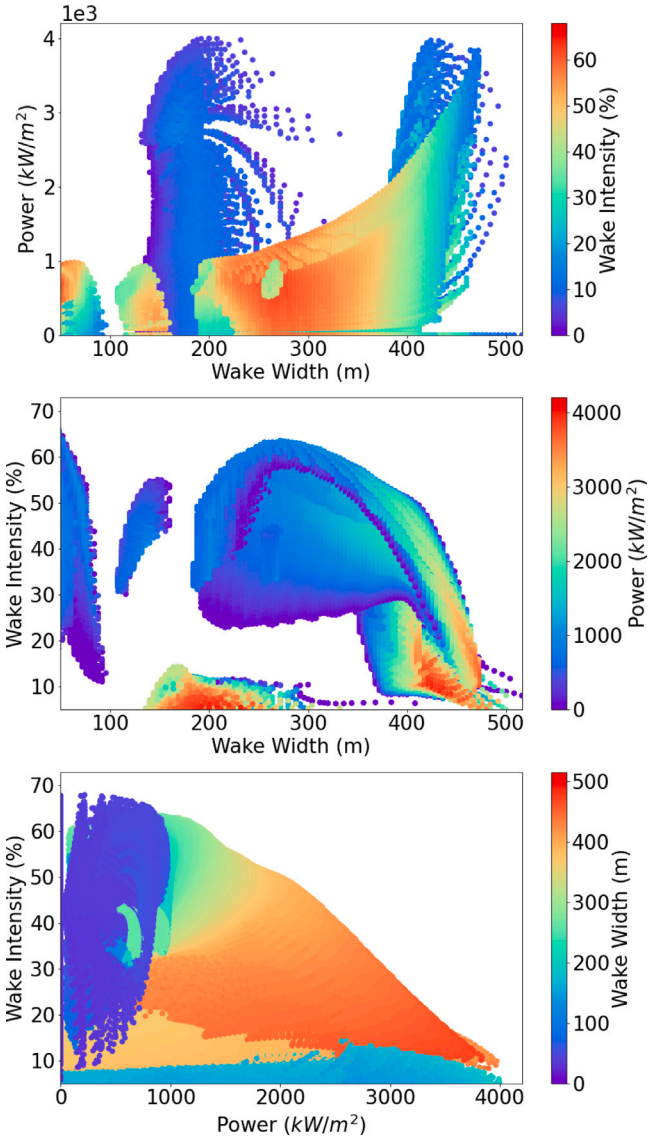

Fig. A.20. Representation of the variable PTO analysis, varying the point cloud according to power, wake width and wake intensity. The points represent all the combinations of B_{PTO}, C_{PTO}, and wave period, for the 5-WEC aligned farm case. The color represents the value, according to the respective color bars.

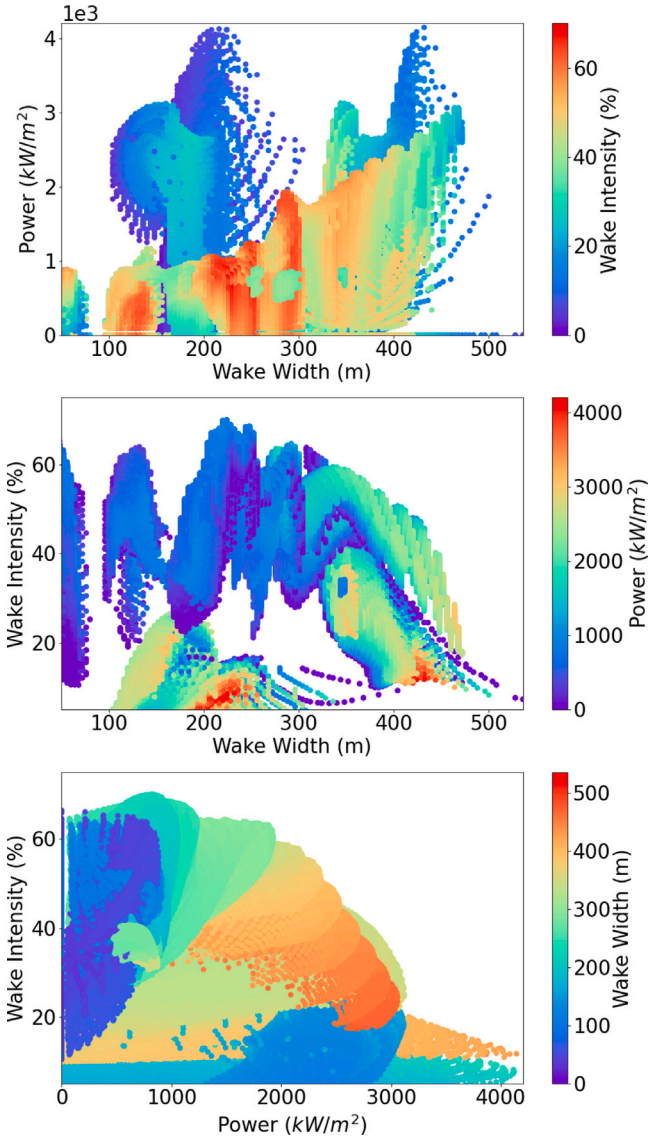

Fig. A.21. Representation of the variable PTO analysis, varying the point cloud according to power, wake width and wake intensity. The points represent all the combinations of B_{PTO}, C_{PTO}, and wave period, for the 5-WEC staggered farm case. The color represents the value, according to the respective color bars.

sheltered sea conditions. Importantly, these outcomes are inherently linked to the specific design of the WEC, and altering the hydrodynamic features of the device could expand its applicability to a broader range of sea sites.

Considering the common practice of deploying WECs in farms to achieve cost-effectiveness, the interactions between devices in the farm may significantly impact the objectives of this study. Various farm layouts, including three and five WECs, in both aligned and staggered configurations, equipped with PTOs, are evaluated. The presence of multiple WECs within the farm contributes to greater perturbations in the wave field, resulting in more pronounced wave disturbance coefficients. However, the specific layout of the farm, the spacing between the WECs, and the utilization of versatile PTOs for each device may exert additional influence on the dynamics. These aspects warrant further exploration, as they can significantly impact the balance between power production and coastal protection. In a broader context, the study underscores the potential for elevating coastal protection to a level of equal importance with power production in the design of WEC farms. Future research may consider selecting a specific real-world coastal location and, in consideration of the site's unique coastal protection requirements, assess the potential for power generation once wave attenuation needs are met. Even if a WEC farm's coastal protection capabilities fall short of meeting minimal requirements, it does not rule out the possibility of a complementary solution. As long as the WEC farm contributes to some degree of wave attenuation, it could be installed in proximity to an existing breakwater or groyne, potentially extending the structure's service life.

In summary, the findings of this study have far-reaching implications for coastal management strategies, suggesting that optimized WEC farm designs and control strategies can provide a sustainable solution for both renewable energy generation and coastal protection. This approach offers coastal regions the opportunity to harness wave energy while concurrently safeguarding their shorelines.

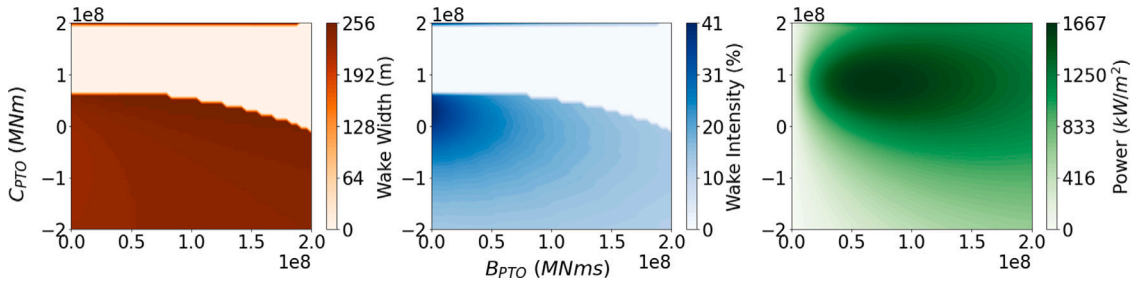

Fig. A.22. Representation of the variable PTO analysis for the 3-WEC staggered farm, at $T = 6$ s. The parameters of interest (wake width, wake intensity, and power) are displayed with different colors, for varying values of B_{PTO} and C_{PTO}.

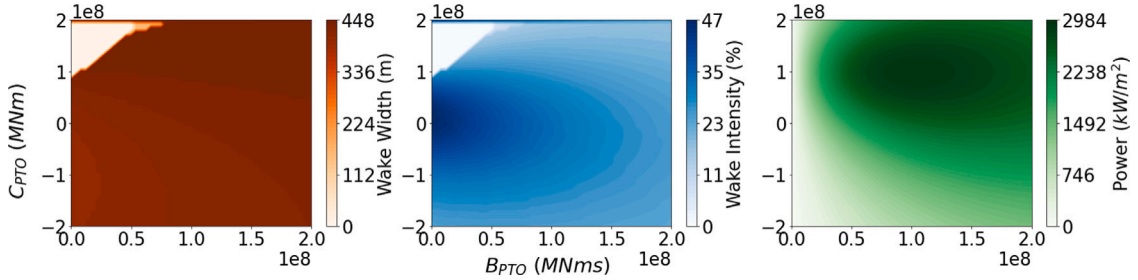

Fig. A.23. Representation of the variable PTO analysis for the 5-WEC aligned farm, at $T = 6$ s. The parameters of interest (wake width, wake intensity, and power) are displayed with different colors, for varying values of B_{PTO} and C_{PTO}.

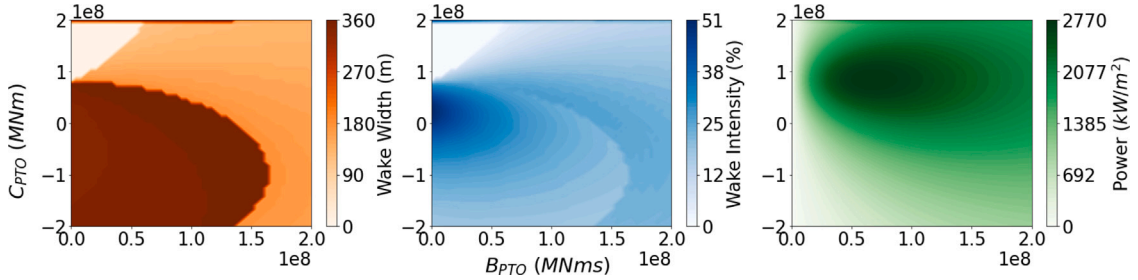

Fig. A.24. Representation of the variable PTO analysis for the 5-WEC staggered farm, at $T = 6$ s. The parameters of interest (wake width, wake intensity, and power) are displayed with different colors, for varying values of B_{PTO} and C_{PTO}.

CRediT authorship contribution statement

Beatrice Battisti: Conceptualization, Methodology, Software, Visualization, Formal analysis, Writing – original draft. **Giuseppe Giorgi:** Conceptualization, Writing – original draft, Supervision. **Gael Verao Fernandez:** Software, Writing – review & editing.

Declaration of competing interest

The authors declare that they have no known competing financial interests or personal relationships that could have appeared to influence the work reported in this paper.

Acknowledgments

This project has received funding from the European Union's Horizon 2020 research and innovation programme under the Marie Skłodowska-Curie grant agreement No: 101068736.

Appendix. Additional farm results

Here, we present supplementary results for the farm scenarios, as an extension to the discussion in Section 5. Specifically, Figs. A.16,A.17 illustrate the alterations in the free surface, with a particular emphasis on the wake, when deploying 5 WECs, arranged both in alignment and staggered configurations, without PTO. Additionally, Fig. A.18 provides the q-factor for the individual OSWCs in the 5-WEC farms. Figs. A.19–A.24 represents the variable PTO analysis for the 3-WEC staggered farm, and the 5-WEC aligned and staggered farms.

References

[1] R. Novo, P. Marocco, G. Giorgi, A. Lanzini, M. Santarelli, G. Mattiazzo, Planning the decarbonisation of energy systems: The importance of applying time series clustering to long-term models, Energy Convers. Manage.: X 15 (January) (2022) 100274, http://dx.doi.org/10.1016/j.ecmx.2022.100274.

[2] K. Kardakaris, I. Boufidi, T. Soukissian, Offshore wind and wave energy complementarity in the greek seas based on ERA5 data, Atmosphere 12 (10) (2021) 1360, http://dx.doi.org/10.3390/ATMOS12101360.

[3] J.L. Villate, P. Ruiz-Minguela, J. Berque, L. Pirttimaa, D. Cagney, C. Cochrane, H. Jeffrey, Strategic Research and Innovation Agenda for Ocean Energy, Technical Report, 2020, URL https://www.oceanenergy-europe.eu/wp-content/uploads/2020/05/ETIP-Ocean-SRIA.pdf.

[4] E. Giglio, E. Petracca, B. Paduano, C. Moscoloni, G. Giorgi, S.A. Sirigu, Estimating the cost of wave energy converters at an early design stage: A bottom-up approach, Sustainability 15 (8) (2023) 6756, http://dx.doi.org/10.3390/SU15086756.

[5] S. Foteinis, T. Tsoutsos, Strategies to improve sustainability and offset the initial high capital expenditure of wave energy converters (WECs), 2016, http://dx.doi.org/10.1016/j.rser.2016.11.258.

[6] M. Penalba, I. Touzón, J. Lopez-Mendia, V. Nava, A numerical study on the hydrodynamic impact of device slenderness and array size in wave energy farms

in realistic wave climates, Ocean Eng. 142 (2017) 224–232, http://dx.doi.org/10.1016/j.oceaneng.2017.06.047.
[7] A. Sinha, D. Karmakar, C. Guedes Soares, Performance of optimally tuned arrays of heaving point absorbers, Renew. Energy 92 (2016) 517–531, http://dx.doi.org/10.1016/J.RENENE.2016.02.043.
[8] C. Beels, P. Troch, J.P. Kofoed, P. Frigaard, J. Vindahl Kringelum, P. Carsten Kromann, M. Heyman Donovan, J. De Rouck, G. De Backer, A methodology for production and cost assessment of a farm of wave energy converters, Renew. Energy 36 (12) (2011) 3402–3416, http://dx.doi.org/10.1016/j.renene.2011.05.019.
[9] H.W. Fang, Y.Z. Feng, G.P. Li, Optimization of wave energy converter arrays by an improved differential evolution algorithm, Energies 11 (12) (2018) 3522, http://dx.doi.org/10.3390/EN11123522.
[10] S. Bozzi, M. Giassi, A. Moreno Miquel, A. Antonini, F. Bizzozero, G. Gruosso, R. Archetti, G. Passoni, Wave energy farm design in real wave climates: the Italian offshore, Energy 122 (2017) 378–389, http://dx.doi.org/10.1016/j.energy.2017.01.094.
[11] M. Göteman, M. Giassi, J. Engström, J. Isberg, Advances and challenges in wave energy park optimization—A review, Front. Energy Res. 8 (2020) 26, http://dx.doi.org/10.3389/fenrg.2020.00026.
[12] H. Abdulkadir, A. Ellithy, O. Abdelkhalik, Heterogeneous WEC array optimization using the hidden genes genetic algorithm, Proc. Eur. Wave Tidal Energy Conf. 15 (2023) http://dx.doi.org/10.36688/ewtec-2023-286.
[13] J.V. Ringwood, S. Zhan, N. Faedo, Empowering wave energy with control technology: Possibilities and pitfalls, Annu. Rev. Control 55 (2023) 18–44, http://dx.doi.org/10.1016/J.ARCONTROL.2023.04.004.
[14] N. Faedo, Y. Peña-Sanchez, E. Pasta, G. Papini, F.D. Mosquera, F. Ferri, SWELL: An open-access experimental dataset for arrays of wave energy conversion systems, Renew. Energy 212 (2023) 699–716, http://dx.doi.org/10.1016/J.RENENE.2023.05.069.
[15] S. Foteinis, Wave energy converters in low energy seas: Current state and opportunities, Renew. Sustain. Energy Rev. 162 (2022) 112448, http://dx.doi.org/10.1016/J.RSER.2022.112448.
[16] K. Kazimierczuk, C. Henderson, K. Duffy, S. Hanif, S. Bhattacharya, S. Biswas, E. Jacroux, D. Preziuso, D. Wu, D. Bhatnagar, B. Tarekegne, A socio-technical assessment of marine renewable energy potential in coastal communities, Energy Res. Soc. Sci. 100 (2023) 103098, http://dx.doi.org/10.1016/J.ERSS.2023.103098.
[17] T. Schoonees, A. Gijón Mancheño, B. Scheres, T.J. Bouma, R. Silva, T. Schlurmann, H. Schüttrumpf, Hard structures for coastal protection, towards greener designs, Estuaries Coasts 42 (7) (2019) 1709–1729, http://dx.doi.org/10.1007/S12237-019-00551-Z/TABLES/3.
[18] D. Khojasteh, A. Shamsipour, L. Huang, S. Tavakoli, M. Haghani, F. Flocard, M. Farzadkhoo, G. Iglesias, M. Hemer, M. Lewis, S. Neill, M.M. Bernitsas, W. Glamore, A large-scale review of wave and tidal energy research over the last 20 years, Ocean Eng. 282 (2023) 114995, http://dx.doi.org/10.1016/J.OCEANENG.2023.114995.
[19] A. Tănase Zanopol, F. Onea, E. Rusu, Coastal impact assessment of a generic wave farm operating in the Romanian nearshore, Energy 72 (2014) 652–670, http://dx.doi.org/10.1016/J.ENERGY.2014.05.093.
[20] A. Mérigaud, B. Thiria, R. Godoy-Diana, Geometrical framework for hydrodynamics and control of wave energy converters, PRX Energy 2 (2) (2023) 023003, http://dx.doi.org/10.1103/PRXEnergy.2.023003.
[21] R.J. Bergillos, A. López-Ruiz, E. Medina-López, A. Moñino, M. Ortega-Sánchez, The role of wave energy converter farms on coastal protection in eroding deltas, guadalfeo, southern Spain, J. Clean. Prod. 171 (2018) 356–367, http://dx.doi.org/10.1016/J.JCLEPRO.2017.10.018.
[22] J. Abanades, D. Greaves, G. Iglesias, Coastal defence using wave farms: The role of farm-to-coast distance, 2014, http://dx.doi.org/10.1016/j.renene.2014.10.048.
[23] N. Tomey-Bozo, A. Babarit, J. Murphy, V. Stratigaki, P. Troch, T. Lewis, G. Thomas, Wake effect assessment of a flap type wave energy converter farm under realistic environmental conditions by using a numerical coupling methodology, Coast. Eng. 143 (2019) 96–112, http://dx.doi.org/10.1016/j.coastaleng.2018.10.008, URL https://www.sciencedirect.com/science/article/pii/S0378383917305549.
[24] P. Balitsky, N. Quartier, V. Stratigaki, G. Verao Fernandez, P. Vasarmidis, P. Troch, Analysing the near-field effects and the power production of near-shore WEC array using a new wave-to-wire model, Water 11 (6) (2019) http://dx.doi.org/10.3390/w11061137, URL https://www.mdpi.com/2073-4441/11/6/1137.
[25] P. Balitsky, G. Bacelli, J. Ringwood, Control-influenced layout optimization of arrays of wave energy converters, 9, 2014, http://dx.doi.org/10.1115/OMAE2014-24136,
[26] P. Garcia Rosa, G. Bacelli, J. Ringwood, Control-informed optimal array layout for wave farms, Sustain. Energy, IEEE Trans. 6 (2015) 575–582, http://dx.doi.org/10.1109/TSTE.2015.2394750.
[27] Y. Peña-Sanchez, D. García-Violini, M. Penalba, A. Zarketa, V. Nava, J. Ringwood, Spectral control co-design of wave energy converter array layout, Proc. Eur. Wave Tidal Energy Conf. 15 (2023) http://dx.doi.org/10.36688/ewtec-2023-531.
[28] B. Zanuttigh, E. Angelelli, Experimental investigation of floating wave energy converters for coastal protection purpose, Coast. Eng. 80 (2013) 148–159, http://dx.doi.org/10.1016/J.COASTALENG.2012.11.007.
[29] G.V. Fernandez, V. Stratigaki, N. Quartier, P. Troch, Influence of power take-off modelling on the far-field effects of wave energy converter farms, Water 13 (4) (2021) 429, http://dx.doi.org/10.3390/W13040429.
[30] R. Bergillos, C. Rodriguez-Delgado, J. Allen, G. Iglesias, Wave energy converter geometry for coastal flooding mitigation, Sci. Total Environ. 668 (2019) 1232–1241, http://dx.doi.org/10.1016/j.scitotenv.2019.03.022.
[31] C. Rodriguez-Delgado, R.J. Bergillos, G. Iglesias, Dual wave farms for energy production and coastal protection under sea level rise, J. Clean. Prod. 222 (2019) 364–372, http://dx.doi.org/10.1016/j.jclepro.2019.03.058.
[32] C. Rodriguez-Delgado, R.J. Bergillos, G. Iglesias, An artificial neural network model of coastal erosion mitigation through wave farms, Environ. Model. Softw. 119 (2019) 390–399, http://dx.doi.org/10.1016/j.envsoft.2019.07.010.
[33] B. Battisti, G. Giorgi, G. Verao Fernandez, P. Troch, A multiquery analysis of a PeWEC farm, Proc. Eur. Wave Tidal Energy Conf. 15 (2023) http://dx.doi.org/10.36688/ewtec-2023-333.
[34] M. Ancellin, F. Dias, Capytaine: A python-based linear potential flow solver, J. Open Source Softw. 4 (36) (2019) 1341, http://dx.doi.org/10.21105/joss.01341.
[35] A. Babarit, G. Delhommeau, Theoretical and numerical aspects of the open source BEM solver NEMOH, in: Proceedings of the 11th European Wave and Tidal Energy Conference, (EWTEC2015), Nantes, France, 2015.
[36] G. Giorgi, N. Faedo, Performance enhancement of a vibration energy harvester via harmonic time-varying damping: A pseudospectral-based approach, Mech. Syst. Signal Process. 165 (2022) 108331, http://dx.doi.org/10.1016/J.YMSSP.2021.108331.
[37] N. Faedo, G. Giorgi, J.V. Ringwood, G. Mattiazzo, Optimal control of wave energy systems considering nonlinear Froude–Krylov effects: control-oriented modelling and moment-based control, Nonlinear Dynam. 109 (3) (2022) 1777–1804, http://dx.doi.org/10.1007/s11071-022-07530-3.
[38] M. Bonfanti, G. Giorgi, Improving computational efficiency in WEC design: Spectral-domain modelling in techno-economic optimization, J. Mar. Sci. Eng. 10 (10) (2022) 1468, http://dx.doi.org/10.3390/JMSE10101468.
[39] J.N. Newman, Marine Hydrodynamics, MIT Press Cambridge, 1977, p. xiii, 402.
[40] G. Giorgi, S. Sirigu, M. Bonfanti, G. Bracco, G. Mattiazzo, Fast nonlinear Froude–Krylov force calculation for prismatic floating platforms: A wave energy conversion application case, J. Ocean Eng. Mar. Energy 7 (4) (2021) 439–457, http://dx.doi.org/10.1007/S40722-021-00212-Z.
[41] A. Rahimi, S. Rezaei, J. Parvizian, S. Mansourzadeh, J. Lund, R. Hssini, A. Düster, Numerical and experimental study of the hydrodynamic coefficients and power absorption of a two-body point absorber wave energy converter, Renew. Energy 201 (2022) 181–193, http://dx.doi.org/10.1016/j.renene.2022.10.103.
[42] V. Sundar, S. Sannasiraj, H. Kaldenhoff, Directional spreading of waves in the nearshore zone, Ocean Eng. 26 (2) (1998) 161–188, http://dx.doi.org/10.1016/S0029-8018(97)00040-1.
[43] M. Penalba, C. Guo, A. Zarketa-Astigarraga, G. Cervelli, G. Giorgi, B. Robertson, Bias correction techniques for uncertainty reduction of long-term metocean data for ocean renewable energy systems, Renew. Energy 219 (2023) 119404, http://dx.doi.org/10.1016/j.renene.2023.119404.
[44] F. Niosi, E. Begovic, C. Bertorello, B. Rinauro, G. Sannino, M. Bonfanti, S. Sirigu, Experimental validation of orcaflex-based numerical models for the PEWEC device, Ocean Eng. 281 (2023) 114963, http://dx.doi.org/10.1016/J.OCEANENG.2023.114963.
[45] J.r. Hals, A. Babarit, A. Kurniawan, T. Moan, The numwec project. Numerical estimation of energy delivery from a selection of wave energy converters – final report, (APRIL) 2011, http://dx.doi.org/10.13140/RG.2.1.3807.8885.
[46] A. Babarit, On the park effect in arrays of oscillating wave energy converters, Renew. Energy 58 (2013) 68–78, http://dx.doi.org/10.1016/j.renene.2013.03.008.